General relativistic simulations of binary black hole-neutron stars: Precursor electromagnetic signals

Vasileios Paschalidis, Zachariah B. Etienne, and Stuart L. Shapiro*
Department of Physics, University of Illinois at Urbana-Champaign, Urbana, IL 61801

We perform the first general relativistic force-free simulations of neutron star magnetospheres in orbit about spinning and non-spinning black holes. We find promising precursor electromagnetic emission: typical Poynting luminosities at, e.g., an orbital separation of $r = 6.6R_{\rm NS}$ are $L_{\rm EM} \sim 6 \times 10^{42}(B_{\rm NS,p}/10^{13}{\rm G})^2({\rm M_{NS}}/1.4{\rm M}_\odot)^2{\rm erg/s}$. The Poynting flux peaks within a broad beam of $\sim 40^\circ$ in the azimuthal direction and within $\sim 60^\circ$ from the orbital plane, establishing a possible lighthouse effect. Our calculations, though preliminary, preview more detailed simulations of these systems that we plan to perform in the future.

PACS numbers: 04.25.D-,04.25.dk,04.30.-w,52.35.Hr

Black hole–neutron star (BHNS) binaries are among the most promising sources for the simultaneous detection of gravitational wave (GW) and electromagnetic (EM) signals in the era of multimessenger astronomy. For example, Advanced LIGO is expected to detect between 1–100 BHNS GW signals each year [1–4]. In addition, BHNS mergers may provide the central engine that powers a short-hard gamma-ray burst (sGRB). GW signals from the inspiral and merger of BHNSs have been computed recently in full general relativity (GR) [5–11], and the first parametric study of magnetized BHNS mergers in full GR has been been carried out in [12, 13], where it was shown that under appropriate conditions BHNSs can launch collimated jets – necessary ingredients for many sGRB models.

Apart from post-merger EM signals, detectable EM pre-merger signals may arise during a BHNS inspiral. Detecting such precursor signals, combined with GW observations, will yield a wealth of information about BHNS binaries. EM signals will help localize the source on the sky, resulting in improved parameter estimation from GWs by eliminating degeneracies resulting form imprecise localization of the source [14].

Neutron stars are believed to be endowed with dipole magnetic fields. Thus, toward the end of a BHNS inspiral, strong magnetic fields will thread and sweep the BH horizon, possibly establishing a unipolar inductor (UI) DC circuit [15] that extracts energy from the system. This exciting new possibility has been suggested recently [16] as a potential mechanism for powering precursor EM signals from BHNSs. Follow-up analytical approximations in the high-mass ratio limit have been performed [16–18] to estimate the total EM output. But, as these UIs operate in strongly curved, dynamical spacetimes, numerical relativity simulations are necessary to reliably determine the amount of EM output, especially in the regime of comparable-mass binaries where previous approximations do not apply. While UIs are not unique to BHNS binaries (they can operate in other types of compact binaries, such as NSNSs [17, 19, 20]), BHNSs may be optimal systems for this mechanism because the azimuthal twist of the magnetic flux tubes is less than unity for a BH resistor [21].

In this Letter we simulate NS magnetospheres in orbit about spinning and nonspinning BHs prior to merger via general relativistic, force-free (GRFF) simulations. We calculate the Poynting luminosity and characterize its angular dependence. In addition, we treat another EM emission mechanism: magnetic dipole (MD) radiation from the accelerating NS. MD radiation has been considered in the context of EM emission affecting the inspiral and GW signal [22], but not as a potential source for strong precursor EM signals. Here we show that the MD Poynting luminosity is significant, and may be the dominant source of EM output in cases where UI does not operate either because of corotation or large values of azimuthal twist of the magnetic flux tubes. We use geometrized units where $c = 1 = G$, unless otherwise stated.

Solving the GRFF equations generally involves evolving the electric ($\mathbf{E}$) and magnetic ($\mathbf{B}$) fields under the force-free constraints $\mathbf{E}\cdot\mathbf{B} = 0$ and $E^2 < B^2$ [23, 24]. The force-free regime represents the limit of ideal MHD when the magnetic fields dominate the plasma dynamics [23, 25]. In this regime one can choose the $\mathbf{B}$-field and the Poynting vector $\mathbf{S}$ as the dynamical variables and cast their evolution equations in conservation form [26, 27]. The force-free constraints then become $\mathbf{S}\cdot\mathbf{B} = 0$ and $S^2 < B^4$ as we show in [27]. One of the greatest advantages of this alternative GRFF formulation is that an ideal GRMHD code can be easily modified to also solve the GRFF equations [26]. The GRFF formulation we adopt here is the same as that in [26], except that at every timestep, in addition to $S^2 < B^4$, we also enforce the algebraic constraint $\mathbf{S}\cdot\mathbf{B} = 0$, which was ignored in [26]. This formulation is embedded in the fully GRMHD in-

* Also at Department of Astronomy and NCSA, University of Illinois at Urbana-Champaign, Urbana, IL 61801

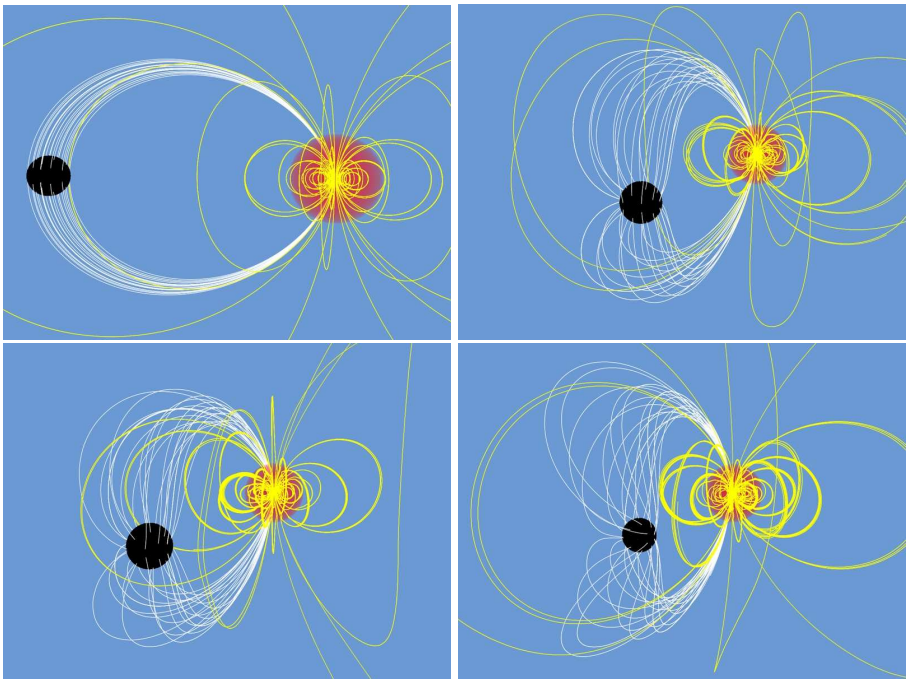

FIG. 1. Initial magnetic field in the nonspinning $a_* = 0$ case (upper left panel). Relaxed magnetic field at $t \approx 1.5$ orbits: $a_* = 0$ (lower left panel), $a_* = -0.5$ (upper right panel), and $a_* = 0.75$ (lower right panel). The black sphere represents the BH horizon and the NS is shown in red. Both white and yellow lines are the magnetic fields lines. White lines distinguish field lines that intersect the BH horizon.

frastructure we presented and tested in [28–30]. In addition, to enforce the $\nabla \cdot \mathbf{B} = 0$ constraint on our adaptive-mesh-refinement grids, the magnetic induction equation is evolved via the vector potential formulation we introduced in [12, 29, 30], coupled to the Generalized Lorenz (GL) gauge condition we devised [13, 30, 31]. We set the damping parameter of GL gauge $\xi = 1.5/\Delta t$, where Δt is the timestep of the coarsest level.

At large separations, the inspiral timescale is much longer than the orbital timescale. So to model the BHNS binary spacetime and the NS matter fields, we adopt quasiequilibrium solutions of the conformal-thin-sandwich (CTS) equations for companions at fixed orbital separation [5, 32, 33]. The CTS approximation is excellent at the separations and BH spins we consider in this work. It also yields a binary spacetime with a helical Killing vector, which enables us to perform the simulations in the center-of-mass frame by simply rotating the spacetime and the fluid rest-mass density and four-velocity in the same fashion as in [34]. This implementation is equivalent to assuming stationary equilibrium of the matter and the gravitational fields in the corotating frame of the binary. The problem is thus reduced to evolving the EM fields ($\mathbf{B}$ and $\mathbf{S}$) in the background matter fields and spacetime.

Given that force-free electrodynamics is a limit of ideal MHD, the *same* ideal MHD evolution equations can be used to evolve both the NS interior and the force-free exterior EM fields, provided in the exterior a compatible force-free velocity is used [26] and the rest-mass density is set to zero. This guarantees a smooth transition from the ideal MHD interior to the force-free exterior, and the MHD variables on the NS surface effectively provide boundary conditions for the exterior force-free evolution. However, given that the chosen initial A-field is not a CTS solution, we evolve the induction equation [Eqs. (8), (9) in [12]] in the NS interior, using the known CTS fluid four-velocity. This sets the boundary condition on the NS surface for the force-free velocity and magnetic field in the exterior. For more details see [27]. Note that after tidal disruption, a GRFF treatment becomes inadequate and must be replaced by full GRMHD.

In addition to our new GRFF evolution techniques, we have also added two new (but equivalent) diagnostics to monitor the outgoing EM luminosity: (i) the ϕ_2 Newman-Penrose scalar [35–37], and (ii) the Poynting vector $\mathbf{S} = (\mathbf{E} \times \mathbf{B})/4\pi$. To compute ϕ_2 we use the same null tetrad as in [38], and the outgoing luminosity is [39]

$$L_{\rm EM} \equiv \lim_{r\to\infty} \frac{1}{4\pi} \int r^2 |\phi_2|^2 d\Omega = \lim_{r\to\infty} \int r^2 S^{\hat{r}} d\Omega. \quad (1)$$

The spacetime and NS initial data we use correspond to cases A, B, C given in Table I in [5]. The BH spin parameters are $a_* \equiv a/M_H = -0.5, 0, 0.75$, and the BH:NS mass ratio is $q = 3$. The CTS NS fluid is modeled as an equilibrium, irrotational, unmagnetized, $\Gamma = 2$ poly-

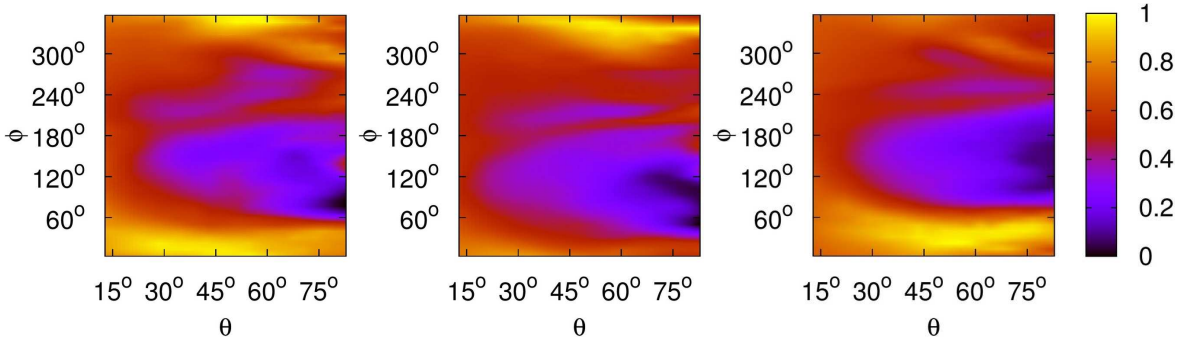

FIG. 2. Angular distribution of Poynting flux, normalized by its peak value on a sphere of radius $120M = 915(M_{\rm NS}/1.4M_\odot)$km. Left: spin -0.5, middle: spin 0, right: spin 0.75. The plots correspond to a time after about 2 orbits.

trope. We seed the initial NS with a purely poloidal magnetic field that approximately corresponds to that generated by a current loop. The coordinate-basis toroidal component of this vector potential is

$$A_\phi = \frac{\pi r_0^2 I_0}{(r_0^2+r^2)^{3/2}}\left(1+\frac{15 r_0^2(r_0^2+\varpi^2)}{8(r_0^2+r^2)^2}\right), \qquad (2)$$

where r_0 is the current loop radius, I_0 the loop current, $r^2=(x-x_{\rm NS})^2+(y-y_{\rm NS})^2+z^2$, $\varpi^2=(x-x_{\rm NS})^2+(y-y_{\rm NS})^2$, and $x_{\rm NS}, y_{\rm NS}$ are the initial coordinates of the NS center of mass. For $r_0 \ll r$ Eq. (2) gives rise to the standard B-field from a current loop on the z-axis, and the characteristic $1/r^3$ fall-off of a standard magnetic dipole on the $z=0$ plane. Choosing $r_0 = R_{\rm NS}/3$ in all our simulations, where $R_{\rm NS}$ is the NS polar radius, we find that the initial magnetic field scales as $1/r^3$ outside the NS to a very good degree. Our simulations are independent of the magnetic field strength. If we set $I_0 = 0.0007$, the initial NS polar magnetic field (as measured by a CTS normal observer) is 8.8×10^{15}G. The initial magnetic field geometry is shown in the upper left panel of Fig. 1.

For the $a_* = 0$ case we perform a resolution study: the low, medium and high resolutions cover the BH horizon radius by 19, 29 and 36 zones, respectively. We also perform the simulations of the $a_* \neq 0$ BH cases using two resolutions, corresponding to the medium and high resolutions of the $a_* = 0$ case. In all simulations we use 9 levels of refinement placing the outer boundary at $400M \approx 3050(M_{\rm NS}/1.4M_\odot)$km, and impose reflection symmetry across the orbital plane.

After a transient phase that lasts a little over 1 orbit, the magnetic field geometry settles into a quasistationary configuration, which we show in Fig. 1. It is evident that in the spinning cases, partial winding of the magnetic field has taken place due to frame dragging, which is most prominent in the $a_* = 0.75$ case.

In Fig. 2 we show the angular distribution of the Poynting flux. In all cases, the Poynting flux peaks within a broad beam of $\sim 40^\circ$ in the azimuthal direction, and in the $a_* = 0$ and $a_* = 0.75$ cases within $\sim 60^\circ$ from the orbital plane. This may establish a lighthouse effect as a characteristic EM signature of BHNS systems prior to merger, if the variation is not washed out by intervening matter.

The time evolution of the computed luminosities is shown in Fig. 3. After a transient period caused by our choice of non-stationary initial magnetic fields, the luminosities settle to an approximately constant value as expected. We find that the time-averaged luminosities after the first 1.5 orbits at the adopted separation are

$$\begin{aligned}
\langle L_{a_*=-0.5}\rangle &= 6.6\times10^{42}\left(\frac{B_{\rm NS,p}}{10^{13}{\rm G}}\right)^2\left(\frac{M_{\rm NS}}{1.4M_\odot}\right)^2 {\rm erg/s},\\
\langle L_{a_*=0}\rangle &= 6.2\times10^{42}\left(\frac{B_{\rm NS,p}}{10^{13}{\rm G}}\right)^2\left(\frac{M_{\rm NS}}{1.4M_\odot}\right)^2 {\rm erg/s},\\
\langle L_{a_*=0.75}\rangle &= 4.8\times10^{42}\left(\frac{B_{\rm NS,p}}{10^{13}{\rm G}}\right)^2\left(\frac{M_{\rm NS}}{1.4M_\odot}\right)^2 {\rm erg/s},
\end{aligned} \qquad (3)$$

where $B_{\rm NS,p}$ is the NS polar magnetic field strength measured by a CTS normal observer, and $M_{\rm NS}$ is the NS rest mass. As the magnetic field inside the NS does not feed back onto the matter evolution, the EM luminosity scales exactly as B^2 for any field strength. The characteristic frequency of this EM radiation is of order the orbital frequency $\sim 200(M_{\rm NS}/1.4M_\odot)^{-1}$Hz at the adopted separation, and hence smaller than typical interstellar-medium plasma frequencies $\sim$ 9kHz. Thus, this radiation will be reprocessed before it reaches the observer.

We now compare our results to the approximate UI formula. The Poynting luminosity of a BHNS UI in the large q limit is given by [16]

$$L_{\rm UI} = \frac{8}{\pi}\left(\frac{r_H}{2M_H}\right)^2 v_{\rm rel}^2 \bar{B}_{\rm NS,p}^2 \left(\frac{R_{NS}}{r}\right)^6 q^2 M_{\rm NS}^2 \qquad (4)$$

where r_H is the horizon radius in units of the BH mass M_H, $\bar{B}_{\rm NS,p}$ is the NS polar magnetic field as measured by zero-angular-momentum observers (ZAMOs) [40], i.e., normal observers in a Kerr spacetime in Boyer-Lindquist coordinates, and r is the binary separation. Here $v_{\rm rel}$ is the azimuthal velocity of magnetic field lines as measured by ZAMOs, for which the following relation was proposed

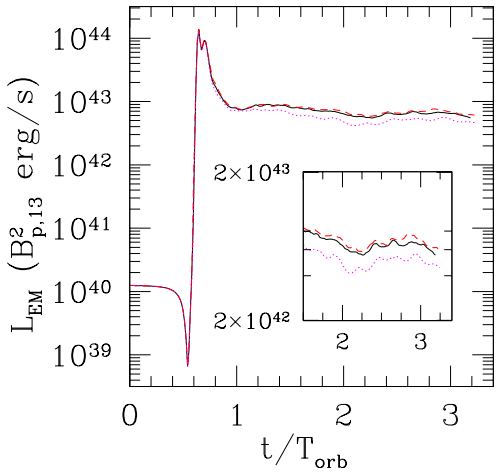

FIG. 3. Poynting luminosity as a function of time calculated on a sphere of radius $120M = 915(M_{\rm NS}/1.4M_\odot)$km for all 3 cases: $a_* = -0.5$ (red) dashed line, $a_* = 0$ (black) solid line, $a_* = 0.75$ (magenta) dotted line. The inset focuses on the last 1.7 orbits of evolution. Here $B_{p,13} = B_{\rm NS,p}/10^{13}$G and $T_{\rm orb}$ is the orbital period.

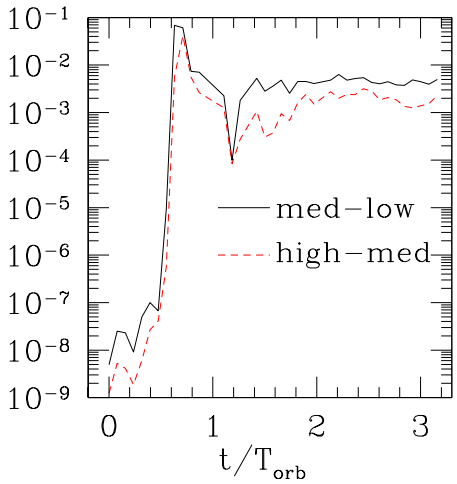

FIG. 4. Convergence of EM luminosity normalized by the maximum luminosity vs. time. The difference between high and medium resolutions is smaller than that between medium and low resolutions, indicating that our scheme is convergent.

[16]: $v_{\rm rel} = r(\Omega - \Omega_{\rm NS}) - \frac{a}{4\sqrt{2}}$, where Ω is the orbital angular frequency, and $\Omega_{\rm NS}$ is the NS spin angular frequency. Given that our BHNS binaries are irrotational, we set $\Omega_{\rm NS} = 0$. Using the binary parameters from our simulations and setting $\bar{B}_{\rm NS,p} \approx B_{\rm NS,p}$ in Eq. (4), we find

$$\begin{aligned} L_{{\rm UI},a_*=0.75} &= 0.12\langle L_{a_*=0.75}\rangle, \\ L_{{\rm UI},a_*=0} &= 0.5\langle L_{a_*=0}\rangle, \\ L_{{\rm UI},a_*=-0.5} &= 0.7\langle L_{a_*=-0.5}\rangle. \end{aligned} \tag{5}$$

Thus, the UI formula seems to predict well the overall magnitude of our computed luminosities. However, in contrast to Eq. (5), which predicts that $L_{{\rm UI},a_*=-0.5}/L_{{\rm UI},a_*=0} \approx 1.5$ and $L_{{\rm UI},a_*=-0.5}/L_{{\rm UI},a_*=0.75} \approx 7.8$, our calculations (3) show only a weak dependence of the Poynting luminosity on the BH spin. This is likely due in part to the spin dependence being added linearly in the proposed formula for $v_{\rm rel}$, and in part to the existence of magnetic dipole emission.

In addition to the UI luminosity, another important EM radiation emission mechanism, that always operates, is that due the accelerating MD moment of the NS. This has been considered previously [22] in the context of EM interactions as they affect the binary inspiral, but not as a mechanism for strong precursor EM counterparts to GWs. The approximate MD luminosity is given by [22]

$$\begin{aligned} L_{\rm EM,MD} \approx 2.4\times10^{41}&\left(\frac{v}{0.3c}\right)^2\left(\frac{B_{\rm NS,p}}{10^{13}{\rm G}}\right)^2 \\ &\left(\frac{M_{\rm NS}}{1.4M_\odot}\right)^2\left(\frac{r}{6.6R_{\rm NS}}\right)^{-6}{\rm erg/s}, \end{aligned} \tag{6}$$

where we inserted parameters from our simulations. $L_{\rm EM,MD}$ is only ~ 20 times smaller than what we observe in our simulations, but is included in our calculated luminosity. MD emission dominates when UI does not operate either because of corotation (and $a_* = 0$ for BHNSs) or because it cannot be established due to the azimuthal twist of the magnetic flux tubes being too large, which may be the case for NSNS binaries [21].

The results of our resolution study in the $a_* = 0$ case are shown in Fig. 4, where it is demonstrated that our scheme is convergent and that the resulting luminosity in the two highest resolutions agree to within $\sim 5\%$. Due to numerical resistivity, the EM energy in the NS interior is conserved after 3 orbits to within 10%, 11%, 7% in the $a_* = -0.5$, $a_* = 0$, $a_* = 0.75$ cases, respectively. Thus, these errors should be taken as the approximate error bars of our calculations.

In a future work we plan to extend our simulations to study the variation of the outgoing Poynting luminosity during the inspiral phase, and its dependence on different mass ratios.

The authors wish to thank Charles F. Gammie, Roman Gold, and Yuk Tung Liu for useful discussions. We also thank the Illinois Relativity Group's REU team [Gregory Colten, Albert Kim, Brian Taylor, and Francis Walsh] for assistance in producing Fig. 1. These visualizations were created using the ZIB Amira software package [41], and we gratefully acknowledge the Zuse Institute Berlin for providing us a license. This paper was supported in part by NSF Grants AST-1002667, and PHY-0963136 as well as NASA Grant NNX11AE11G at the University of Illinois at Urbana-Champaign. This work used the Extreme Science and Engineering Discovery Environment (XSEDE), which is supported by NSF grant number OCI-1053575.

[1] B. Abbott and the LIGO Scientific Collaboration, Phys. Rev. D **77**, 062002 (Mar. 2008)

[2] D. A. Brown, S. Babak, P. R. Brady, N. Christensen, T. Cokelaer, J. D. E. Creighton, S. Fairhurst, G. Gonzalez, E. Messaritaki, B. S. Sathyaprakash, P. Shawhan, and N. Zotov, Class. Quant. Grav. **21**, S1625 (Oct. 2004)

[3] V. Kalogera, K. Belczynski, C. Kim, R. O'Shaughnessy, and B. Willems, Phys. Rept. **442**, 75 (Apr. 2007)

[4] J. Abadie, B. P. Abbott, R. Abbott, M. Abernathy, T. Accadia, F. Acernese, C. Adams, R. Adhikari, P. Ajith, B. Allen, and et al., Classical and Quantum Gravity **27**, 173001 (Sep. 2010)

[5] Z. B. Etienne, Y. T. Liu, S. L. Shapiro, and T. W. Baumgarte, Phys. Rev. D **79**, 044024 (Feb. 2009)

[6] M. D. Duez, F. Foucart, L. E. Kidder, C. D. Ott, and S. A. Teukolsky, Class.Quant.Grav. **27**, 114106 (2010), arXiv:0912.3528 [astro-ph.HE]

[7] F. Foucart, M. D. Duez, L. E. Kidder, and S. A. Teukolsky, Phys.Rev. **D83**, 024005 (2011), arXiv:1007.4203 [astro-ph.HE]

[8] K. Kyutoku, H. Okawa, M. Shibata, and K. Taniguchi, Phys.Rev. **D84**, 064018 (2011), arXiv:1108.1189 [astro-ph.HE]

[9] B. D. Lackey, K. Kyutoku, M. Shibata, P. R. Brady, and J. L. Friedman, Phys.Rev. **D85**, 044061 (2012), arXiv:1109.3402 [astro-ph.HE]

[10] F. Foucart, M. B. Deaton, M. D. Duez, L. E. Kidder, I. MacDonald, *et al.*(2012), arXiv:1212.4810 [gr-qc]

[11] G. Lovelace, M. D. Duez, F. Foucart, L. E. Kidder, H. P. Pfeiffer, *et al.*(2013), arXiv:1302.6297 [gr-qc]

[12] Z. B. Etienne, Y. T. Liu, V. Paschalidis, and S. L. Shapiro, Phys. Rev. D **85**, 064029 (Mar. 2012)

[13] Z. B. Etienne, V. Paschalidis, and S. L. Shapiro, Phys. Rev. D **86**, 084026 (Oct. 2012), arXiv:1209.1632 [astro-ph.HE]

[14] S. Nissanke, M. Kasliwal, and A. Georgieva(2012), arXiv:1210.6362 [astro-ph.HE]

[15] P. Goldreich and D. Lynden-Bell, Astrophys. J. **156**, 59 (Apr. 1969)

[16] S. T. McWilliams and J. Levin, Astrophys. J. **742**, 90 (Dec. 2011), arXiv:1101.1969 [astro-ph.HE]

[17] M. Lyutikov, Phys.Rev. **D83**, 124035 (2011), arXiv:1104.1091 [astro-ph.HE]

[18] D. J. D'Orazio and J. Levin, ArXiv e-prints(Feb. 2013), arXiv:1302.3885 [astro-ph.HE]

[19] A. L. Piro, Astrophys. J. **755**, 80 (Aug. 2012), arXiv:1205.6482 [astro-ph.HE]

[20] C. Palenzuela, L. Lehner, M. Ponce, S. L. Liebling, M. Anderson, *et al.*(2013), arXiv:1301.7074 [gr-qc]

[21] D. Lai, Astrophys. J. Lett. **757**, L3 (Sep. 2012), arXiv:1206.3723 [astro-ph.HE]

[22] K. Ioka and K. Taniguchi, Astrophys.J.(2000), arXiv:astro-ph/0001218 [astro-ph]

[23] S. Komissarov, Mon.Not.Roy.Astron.Soc. **336**, 759 (2002), arXiv:astro-ph/0202447 [astro-ph]

[24] C. Palenzuela, T. Garrett, L. Lehner, and S. L. Liebling, Phys. Rev. D **82**, 044045 (Aug. 2010), arXiv:1007.1198 [gr-qc]

[25] J. C. McKinney and C. F. Gammie, Astrophys.J. **611**, 977 (2004), arXiv:astro-ph/0404512 [astro-ph]

[26] J. C. McKinney, Mon. Not. Roy. Astron. Soc. **367**, 1797 (Apr. 2006), arXiv:astro-ph/0601410

[27] V. Paschalidis, B. E. Zachariah, and L. S. Shapiro, In preparation(2013)

[28] M. D. Duez, Y. T. Liu, S. L. Shapiro, and B. C. Stephens, Phys.Rev. **D72**, 024028 (2005), arXiv:astro-ph/0503420 [astro-ph]

[29] Z. B. Etienne, Y. T. Liu, and S. L. Shapiro, Phys.Rev. **D82**, 084031 (2010), arXiv:1007.2848 [astro-ph.HE]

[30] Z. B. Etienne, V. Paschalidis, Y. T. Liu, and S. L. Shapiro, Phys. Rev. D **85**, 024013 (Jan. 2012)

[31] B. D. Farris, R. Gold, V. Paschalidis, Z. B. Etienne, and S. L. Shapiro, Phys.Rev.Lett. **109**, 221102 (2012), arXiv:1207.3354 [astro-ph.HE]

[32] K. Taniguchi, T. W. Baumgarte, J. A. Faber, and S. L. Shapiro, Phys.Rev. **D72**, 044008 (2005), arXiv:astro-ph/0505450 [astro-ph]

[33] T. W. Baumgarte and S. L. Shapiro, *Numerical Relativity: Solving Einstein's Equations on the Computer* (Cambridge University Press, 2010)

[34] B. D. Farris, Y. T. Liu, and S. L. Shapiro, Phys.Rev. **D84**, 024024 (2011), arXiv:1105.2821 [astro-ph.HE]

[35] E. Newman and R. Penrose, Journal of Mathematical Physics **3**, 566 (May 1962)

[36] S. A. Teukolsky, Astrophys.J. **185**, 635 (1973)

[37] C. Palenzuela, T. Garrett, L. Lehner, and S. L. Liebling, Phys.Rev. **D82**, 044045 (2010), arXiv:1007.1198 [gr-qc]

[38] P. Moesta, D. Alic, L. Rezzolla, O. Zanotti, and C. Palenzuela, Astrophys.J. **749**, L32 (2012), arXiv:1109.1177 [gr-qc]

[39] Notice the factor of $1/4\pi$, which was omitted in [38]. This factor results from the choice of null tetrad. A similar factor of $1/2\pi$ was used in the $L_{\rm EM}$ formulae reported in [36, 37] where a different null tetrad was used.

[40] K. S. Thorne, R. H. Price, and D. A. MacDonald, *Black Holes: The Membrane Paradigm* (1986)

[41] D. Stalling, M. Westerhoff, and H.-C. Hege, in *The Visualization Handbook; Amira: A Highly Interactive System for Visual Data Analysis*, edited by C. D. Hansen and C. R. Johnson (Elsevier, 2005) Chap. 38, pp. 749–767, ISBN 978-0-12-387582-2